

Department of Physics, Chemistry & Biology (IFM)  
Functional Electronics Materials

Jan Eric Stehr  
CAMPUS VALLA  
58183 LINKÖPING  
SWEDEN

# ÅForsk final report 2018-12-31 Grant No. 15-433

## **Novel defect engineered nanowire gas sensors with enhanced sensitivity and functionality**

### **Purpose and Aims:**

ZnO nanowires (NWs) are currently considered among the most attractive material systems for gas and chemical sensing. Performance of these sensors is, however, largely affected by intrinsic defects and impurities present in the material and conditions of the NW surface. In this project we explore deliberate defect and surface engineering to enhance performance and functionality of ZnO-based nanosensors.

The specific objectives of the project are:

- (i) to evaluate effects of specific defects and impurities on electrical and optical properties of ZnO NWs by introducing them in a controlled manner;
- (ii) based on the gained knowledge, to enhance sensitivity and achieve desired gas selectivity by utilizing defect engineering and plasmonic effects.

## Research results:

We have followed the planned activity and found answers for the main objectives of the project. Results related to the project were presented at international conferences and published in peer-reviewed international journals.

Structural, optical and defect properties of ZnO NWs grown by several common growth techniques, including hydrothermal methods, rapid thermal chemical vapor deposition (RTCVD) and carbo-thermal reduction vapor phase transport (VPT). Afterwards the NWs were subjected to thermal annealing in order to deliberately alter the defect and impurity concentrations in the samples. Subsequently, the samples were examined by the means of optically detected magnetic resonance (ODMR) and electron paramagnetic resonance (EPR) complemented by photoluminescence (PL) and scanning electron microscopy (SEM) measurements.

Representative scanning electron microscopy (SEM) images of the hydrothermally as-grown and N-implanted NWs are shown in Figure 1(a) and (b), respectively, with magnified areas shown in Figure 1(d) and (f). Cross sectional SEM images of the as-grown and N-implanted ZnO NWs are depicted in Figure 1(c) and (e), respectively. The NWs form a dense array, have diameters ranging from 60 to 200 nm and a length of around 3  $\mu\text{m}$ . Even after implantation, the NWs remain vertically oriented, though some of them are found to be randomly tilted with angles up to 15°.

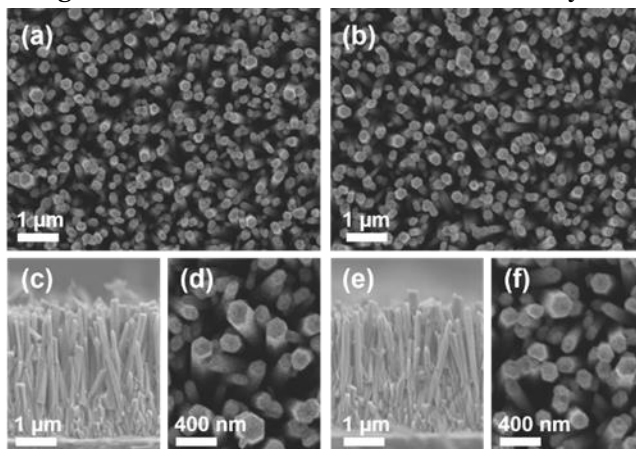


Figure 1: SEM images of the as-grown (a) and N-implanted (b) ZnO NWs. Cross sectional SEM images of the as-grown (c) and N-implanted (e) ZnO NWs. (d) and (f) depict the as-grown and N-implanted ZnO NWs at higher magnification, respectively.

Figure 2 depicts a typical PL spectrum of the as grown ZnO NWs measured at 5 K. In the near-band-edge (NBE) spectral emission range it is dominated by transitions stemming from neutral donor bound excitons ( $D_0X$ ), free excitons (FX) and their phonon replicas (FX-LO) – see the inset in Fig. 2 for a close-up of the PL spectrum within the NBE spectral region. In addition, the spectrum contains a broad PL band that peaks at around 1.9 eV. This red emission is related to the presence of intrinsic defects in ZnO, most likely zinc vacancies. After N implantation one can see that two additional PL bands are appearing in the visible spectral range, the first one is rather weak and peaks around 2.2 eV, which could be attributed to the presence of

oxygen vacancies. The second band peaks at lower energies (~1.75 eV) and indicates the presence of additional deep defects after N-implantation, which could be related to zinc interstitials. In the NBE spectral range N-implantation leads to the appearance of another peak at slightly lower energy than the DOX peak. A similar peak was observed by Ton-That et al. in ZnO NWs annealed in nitrogen plasma and assigned to a neutral acceptor bound ( $A_0X$ ) exciton related to nitrogen. In addition to these additional PL bands, the overall PL intensity was lower by a factor of 15 in the N-implanted ZnO NWs compared to the as-grown ZnO NWs, which was likely caused by implantation damage.

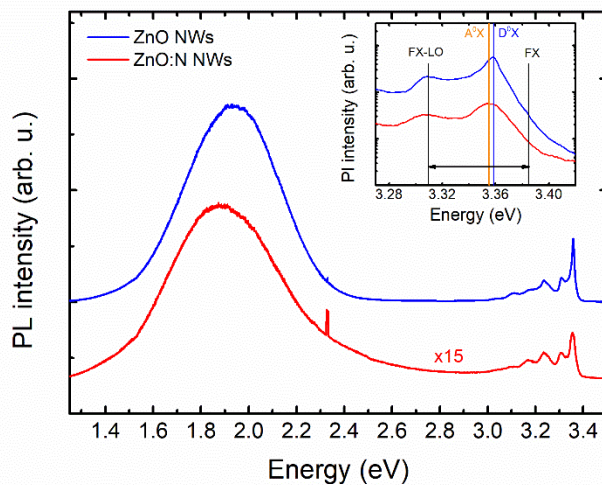


Figure 2: A typical PL spectrum measured at 5 K of as-grown and N-implanted ZnO NWs. The spectra are displayed in the linear scale and offset for clarity. The inset depicts a close-up of the PL spectra within the NBE spectral region, shown in semi-logarithmic scale.

EPR spectra were analyzed using the following spin-Hamiltonian that includes an electron Zeeman term, a central hyperfine interaction term and a fine structure term:

$$\mathcal{H} = \mu_B \mathbf{B} g \mathbf{S} + \mathbf{S} \mathbf{D} \mathbf{S} + \mathbf{S} \mathbf{A} \mathbf{I} . \quad (1)$$

Here,  $\mathbf{S}$  denotes an effective electron spin,  $\mathbf{I}$  the nuclear spin and  $\mathbf{B}$  is an external magnetic field.  $g$  and  $\mathbf{A}$  are the electron  $g$ -tensor and the hyperfine interaction tensor, respectively and  $\mu_B$  is the Bohr magneton. The fine structure splitting for  $S > 1/2$  is described by the tensor  $\mathbf{D}$ . The spin-Hamiltonian parameters obtained from fitting the experimental data are summarized in Table I, together with the parameters of N-related acceptors reported in the literature. Figure 3 shows EPR spectra of the as-grown (b) and N-implanted (a) ZnO NWs measured in the dark  $\mathbf{B} \parallel \mathbf{c}$  and a microwave frequency of 9.4 GHz (X-band). In both structures the spectra contain a broad feature located at around 335 mT with the  $g$ -factor of  $\sim 2.0023$ . This EPR signal can be attributed to surface dangling bonds. Its observation in the studied NWs reflects a large surface-to-volume ratio in the structures. In the range of magnetic fields typical for shallow donors ( $\sim 343$  mT) the as-grown ZnO NWs also exhibit at 10 K an EPR signal consisting of one single line ( $S=1/2$ ) with the  $g$  factor of  $\sim 1.96$  –labeled as SD in Figure 3(a). Such a signal is characteristic for shallow

donors in ZnO. Since the signal can be detected in the dark, the Fermi level ( $E_F$ ) in the as-grown ZnO NWs must be located above the donor level, i.e. close to the conduction band. The shallow donor signal, however, can no longer be detected in the dark after N-implantation, which indicates the formation of compensating acceptors leading to the downshift of  $E_F$ . Furthermore two new EPR signals are detected in the ZnO:N NWs.

The first one, labeled as X in Figure 3(a), contains three features: a positive (negative) line at the low (high) magnetic field and a middle line with a derivative lineshape. Such spectrum is typical for a paramagnetic center with an effective electron spin  $S=1$  in a powder-like system. Consistently, both the splitting between the lines and their lineshape are found to be independent of the microwave frequency (9.4 GHz vs 33 GHz) utilized during the experiments. The best fit to the experimental data can be obtained assuming that the X-center is randomly oriented in the x-y plane (i.e. in the plane orthogonal to the NW growth direction), which likely reflects random rotation of NWs within this plane, evident in the SEM images shown in Figure 1.

The second signal, labeled as N in Figure 3(a), contains three sharp equidistant lines with the derivative lineshape. The splitting between the lines remain the same at different microwave frequencies as seen from Figures 3(a) and 3(c), which show EPR spectra measured at X-band and Q-band, respectively. This rules out the possibility that the lines arise from three different defects with  $S=1/2$  but slightly different g-values. Instead, the N-center can only be described by assuming a resolved hyperfine interaction with a nuclear spin ( $I=1$ ) with almost 100% natural abundance. Nitrogen is the only element that fulfills these criteria, since the  $^{14}\text{N}$  isotope has  $I = 1$  and 99.6% natural abundance. In order to gain further insight into the structure of the center, angular dependent EPR studies were performed by rotating from  $B \parallel c$  to  $B \perp c$ . The corresponding positions of the EPR lines are shown by the open circles in Figure 3(d), whereas Figure 3(e) depicts an experimental spectrum measured in Q-band with  $B \perp c$ . Simulations of the angular-dependent data by using the spin Hamiltonian in Eq.1 yields the set of parameters given in Table I. The results of these simulations are shown by the solid lines in Figure 3(d), as well as by the dashed line (4) in Figure 3(e), where the simulated EPR spectrum for  $B \perp c$  is displayed together with the simulated spectra of other detected EPR signals. Very good agreement between the experimental data and simulation results is observed, justifying validity of the performed analysis. The N-center is found to exhibit an anisotropic behavior of the g-factor and the hyperfine interaction parameter (see Table I). The anisotropy of the g-value, with a positive deviation from the free-electron g-value of 2.0023, proves that this defect is an acceptor type.

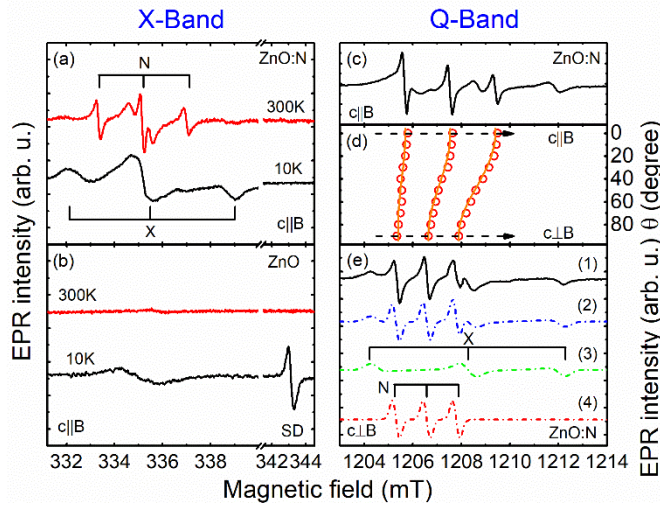


Figure 3: X-Band EPR spectra of the as-grown ZnO NWs (b) and ZnO:N NWs (a) measured in the dark at 10K and 300K with  $B \parallel c$ . (c) Q-Band EPR spectrum of the ZnO:N NWs measured at RT with  $B \parallel c$ . (d) The EPR signal from the N-center as a function of the angle  $\theta$  between  $B$  and  $c$ . The open circles represent experimental positions of the EPR lines, whereas the solid lines are simulation results using the spin-Hamiltonian in Eq.1 with the parameters given in Table I. (e) Q-Band EPR spectrum of the ZnO:N NWs (1) measured at RT with  $B \perp c$  under white-light illumination. The EPR spectra of the X- and N-center simulated by using Eq.1 are depicted by (3) and (4), respectively. (2) shows the sum of (3) and (4).

Next, we exposed the ZnO NW structures to ethanol vapor and measured their PL spectra. Figure 4 shows typical PL spectra of the investigated ZnO NW structures with and without being exposed to ethanol gas. One can clearly see that exposure to ethanol gas substantially quenches the PL emission in the visible spectral range which is caused by defects. This quenching is most likely caused by surficial non-radiative recombining defects created by reaction between the ethanol vapor and the ZnO NWs. Since the quenching is of a substantial amount it is easily possible to detect ethanol vapor with different concentrations.

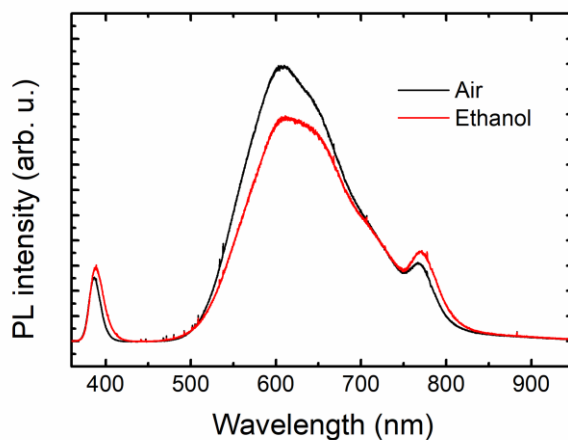


Figure 4: Typical RT PL spectra of ZnO NWs being exposed to air and ethanol.

Next we evaluated if the sensitivity of the ZnO NWs to ethanol vapor can be enhanced by defect incorporation by N ion implantation and thermal treatment (TT) in N<sub>2</sub> atmosphere at 750 °C of the as grown and N implanted (ZnO:N) NWs. After N implantation, which causes mainly the formation of the N-center and zinc interstitials, the sensitivity to ethanol vapor is enhanced by 100% compared to the as grown ZnO NWs (see Figure 5). Thermal treatment of, both, the as-grown and N-implanted ZnO NWs on the other hand decreases the sensitivity to ethanol vapor. In both cases the defects observed in the ZnO NWs after thermal annealing have been altered strongly. This indicates that defects have a strong influence on the sensitivity of ZnO NWs to ethanol vapor. In both thermally treated samples the N-center has vanished after annealing, which is an indication that the N-center could be the origin of the enhanced ethanol sensitivity in ZnO:N NWs.

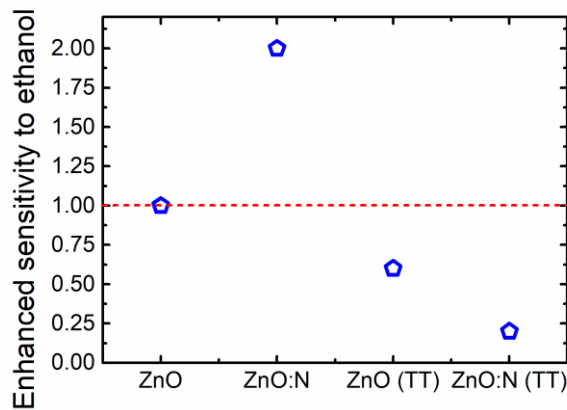


Figure 5: Enhanced sensitivity to ethanol of different ZnO NWs structures normalized to the as-grown ZnO NWs.

In summary, ZnO NWs grown with different growth techniques that were treated by different post-growth treatments, like N-ion implantation and thermal annealing, were studied by SEM, PL, and magnetic resonance spectroscopy. Different defects and impurities were identified in the ZnO NWs depending on the used growth technique and post-growth treatment methods. After ion implantation with N ions a 100% increase in sensitivity to ethanol vapor could be detected, which could be related to the formation of the N-center in the ZnO NWs.

**Table I:** Summary of the spin-Hamiltonian parameters of the defects discussed in this work. The axial components of the electron **g**-tensor are denoted as  $g_{\perp}$  and  $g_{\parallel}$ , while the components for the non-axial centers are given by  $g_x$ ,  $g_y$  and  $g_z$ . For the non-axial centers,  $\varphi$  is the angle between the **z** and **c** axis.

Center	S	I	$g_x$ ( $g_{\perp}$ )	$g_y$	$g_z$ ( $g_{\parallel}$ )	$\varphi$ (deg)
$V_{Zn}^-$ (axial)	1/2		2.0193		2.0041	

$V_{Zn^-}$ (non-axial)	1/2		2.0173	2.0183	2.0041	110.75
$V_{Zn}/Zn_i$	1		1.9888	1.9893	1.9816	110.75
B	1/2			2.007	2.007	
$V_{O^+}$	1/2			1.9960	1.9945	
X-center	1			2.004	2.0035	
N-center	1/2	1		2.0069	2.0054	
$N_{O^0}$	1/2	1		1.963	1.996	
$Zn_i$	1/2			1.9595	1.9605	
EM	1/2			1.955	1.957	
$D^*$	1/2			1.9565	1.9605	

**Publications related to the project (between 01/2016 and 12/2018):**

- J.E. Stehr, W.M. Chen, N.K. Reddy, C.W. Tu, and I.A. Buyanova: Unintentional nitrogen incorporation in ZnO nanowires detected by electron paramagnetic resonance spectroscopy. *physica status solidi (c)*, **13**, 572 (2016).
- J.E. Stehr, S.L. Chen, W.M. Chen, L. Cai, S. Shen, and I.A. Buyanova Identification of an N-related acceptor in ZnO nanowires. (2018) submitted
- J.E. Stehr, S.L. Chen, W.M. Chen, L. Cai, S. Shen, and I.A. Buyanova Effects of N implantation on defect formation in ZnO nanowires. (2018) submitted

**The following topics related to the project were presented at international conferences (between 01/2016 and 12/2018):**

- Energy, Materials & Nanotechnology (EMN) Meeting Prague, Czech Republic, June 21-24, 2016  
Defect properties of ZnO nanowires (poster)  
J. E. Stehr, C. Gray, E. McGlynn, W. M. Chen, and I. A. Buyanova
- Gordon Research Conference: Defects in Semiconductors, New London, NH, USA, August 21-24, 2016  
The Zinc Vacancy-Donor Complex: A Relevant Compensating Center in n-type ZnO (invited talk)  
J. E. Stehr
- International Conference on Superlattices Nanostructures and Nanodevices (ICSNN), Madrid, Spain, July 23-27, 2018  
Effects of N implantation on defect formation in ZnO nanowires (poster)  
J. E. Stehr, W. M. Chen, S. Shen and I. A. Buyanova

In addition, another journal article related to the project is in preparation.